Cryogenics 117 (2021) 103323

Contents lists available at ScienceDirect

Cryogenics

journal homepage: www.elsevier.com/locate/cryogenics

The effects of inclination on a two stage pulse tube cryocooler for use with a ground based observatory

Tran Tsan [a,*], Nicholas Galitzki [a], Aamir M. Ali [b], Kam Arnold [a], Gabriele Coppi [c], Tamar Ervin [d], Logan Foote [b], Brian Keating [a], Jack Lashner [e], John Orlowski-Scherer [f], Michael J. Randall [a], Joseph Seibert [a], Jacob Spisak [a], Grant P. Teply [a], Zhilei Xu [f,g], Ningfeng Zhu [f]

[a] Department of Physics, University of California, San Diego, La Jolla, CA 92093, USA
[b] Department of Physics, University of California, Berkeley, Berkeley, CA 94720, USA
[c] Department of Physics, University of Milano-Bicocca Piazza della Scienza, Milano, MI, Italy
[d] Department of Physics and Astronomy, University of California, Los Angeles, Los Angeles, CA 90024, USA
[e] Department of Physics and Astronomy, University of Southern California, Los Angeles, CA 90089, USA
[f] Department of Physics and Astronomy, The University of Pennsylvania, Philadelphia, PA 19104, USA
[g] MIT Kavli Institute for Astrophysics and Space Research, Massachusetts Institute of Technology, Cambridge, MA 02139, USA

ARTICLE INFO

Keywords:
Pulse Tube Cryocooler
Cryogenic
Angular dependence

ABSTRACT

Ground-based observatories across a wide range of wavelengths implement cryogenic cooling techniques to increase the sensitivity of instruments and enable low temperature detector technologies. Commercial pulse tube cryocoolers (PTCs) are frequently used to provide 40 K and 4 K stages as thermal shells in scientific instruments. However, PTC operation is dependent on gravity, giving rise to changes in cooling capacity over the operational tilt range of pointed telescopes. We present a study of the performance of a two stage PTC with a cooling capacity of 1.8 W at 4.2 K and 50 W at 45 K (Cryomech PT420-RM) from 0 −55° away from vertical to probe capacity as a function of angle over a set of realistic thermal loading conditions. Our study provides a method to extract temperature estimates given predicted thermal loading conditions across the angular range sampled. We then discuss the design implications for current and future tilted cryogenic systems.

1. Introduction

The pulse tube cryocooler (PTC) has evolved significantly from its original design in 1963, as built by Gifford and Longsworth[1], to the current commercially available multi-stage PTCs. The basic components of a PTC include a compressor, a regenerator, and a pulse tube with a heat exchanger at each end of the tube. The PTC operates in a closed and regenerative cycle through adiabatic compression and expansion processes. Unlike the Stirling cryocooler and the Gifford–McMahon (GM) cryocooler, which use a mechanical displacer to carry out the adiabatic process, the PTC uses the residential gas in the pulse tube as a displacer, reducing the number of moving components [2].

The gas goes through two main heat transfers inside the pulse tube: it deposits heat through the heat exchanger at the hot end during the compression, and it absorbs the heat from the cold end during the expansion. As a result, the test sample at the cold end experiences a decrease in temperature. The cycle repeats until it reaches the unit's base cryogenic temperature. More detailed explanations of pulse tube operation can be found in Radebaugh (1999) [2] and Raj et al. (2013) [3].

The gas in the pulse tube is subject to heat transfer by convection that occurs in fluids. In the normal operating mode at vertical orientation the gas column reaches an equilibrium with a thermal gradient from the top to the bottom of the gas column and minimal convective mixing.

Once the PTC is tilted, convective processes can disrupt the thermal gradient, which can reduce the efficiency of the cooling cycle [2]. Therefore, the performance of a PTC is tied to the tilt angle of the system relative to the gravity vector, such that the cooling capacity of the PTC decreases as a function of the tilt angle. This convective effect in PTCs has been studied before [4–6], with efforts to mitigate the effect focusing on high frequency Stirling-type pulse tube (∼ 40 Hz) for space-based applications [7,8]. However, the impact of tilt angle on low frequency two-stage pulse tube systems (∼ 1.4 Hz) has not been extensively explored.

* Corresponding author at: Physics Department, UC San Diego, 9500 Gilman Drive SERF Building Room 460, La Jolla, CA 92093-0424, USA.
E-mail address: ttsan@ucsd.edu (T. Tsan).

https://doi.org/10.1016/j.cryogenics.2021.103323
Received 23 February 2021; Received in revised form 18 June 2021; Accepted 20 June 2021
Available online 27 June 2021

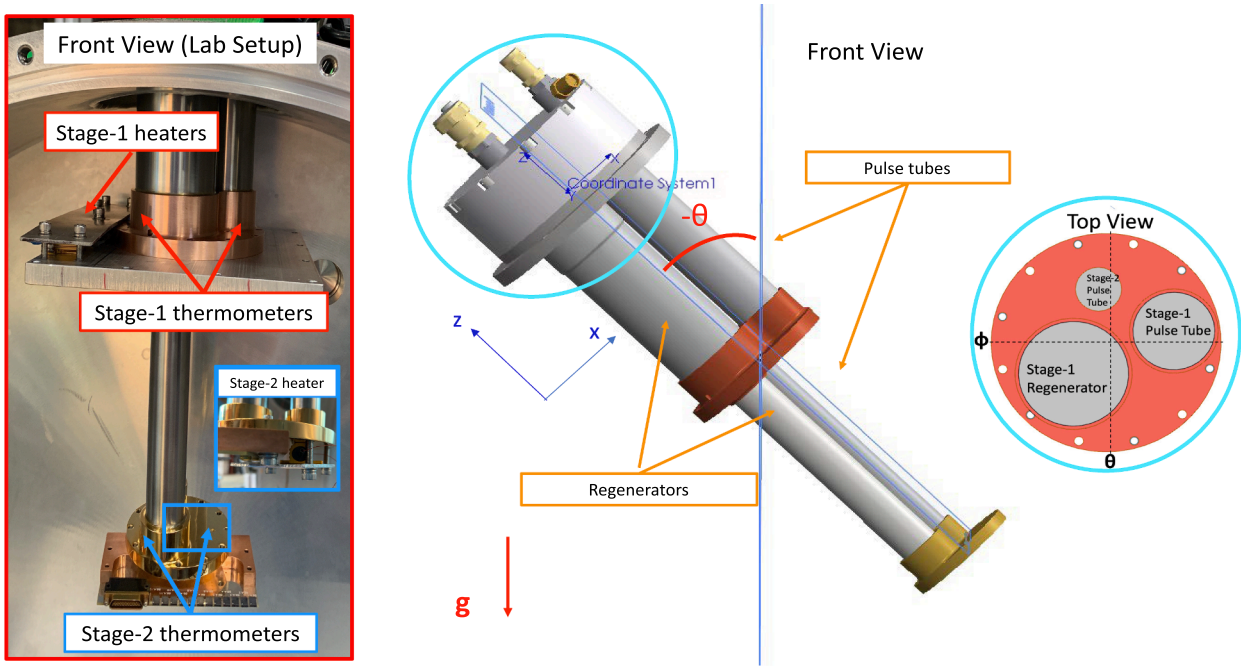

Fig. 1. Experimental setup in lab showing the diodes, heaters, and the rotation of the PTC for various tilt tests. The right picture portrays the negative angle ($-\theta$) tilt tests, with the positive angle ($+\theta$) rotating the other way. We also rotate at an axis perpendicular to the θ axis, ϕ, as a parity check to the orientation effect on the PTC. The top right cutout illustrates the rotation axis for both θ and ϕ. The left picture is a zoom in picture of the thermometry and heater setup on both stages. The breakout were as follow: a 20 Ω heater bank and 2 diodes on the first stage and 500 Ω heater and 2 diodes on the second stage.

We examine the gravitational effect on a two-stage pulse tube cryocooler, operating at 1.4 Hz, through a series of tilt tests. The results are of potential interest to systems that mount PTCs at an angle, especially PT-420 units, which includes a number of upcoming millimeter experiments such as the Simons Observatory (SO) [9,10], CCAT-prime [11], and CMB-S4 [12].

Section 2 describes the experimental setup that was built to test pulse tube performance and our data reduction process. Section 3 provides an analysis of the angular dependence of the pulse tube performance and an empirical model to allow projected performance given loading and angle parameters. We discuss implications for instrument design and potential future work in section 4.

2. Test setup & Methodology

We developed a series of tests at the University of California, San Diego (UCSD) to characterize the pulse tube behavior under different tilt conditions. We recorded the temperature of each of the PTC cold head stages over a range of angles from 0° to 55° with respect to gravity and over a range of thermal loading conditions, from 0 to 51 W and 0 to 1.8 W on the first and second stages, respectively.

2.1. Pulse tube selection

The test used a Cryomech PT-420 [1] model, which was dictated by the available resources at the time. The specific PTC option we used for this experiment was a Cryomech PT-420 with the remote motor variation (PT420-RM) coupled to a CPA1114 Compressor, which has an advertised cooling power of 50 W at 45 K (stage 1) and 1.8 W at 4.2 K (stage 2). We focus on results obtained with a specific pulse tube, hereafter PT420–1, which has a manufacture certified performance at 50 Hz and 260 psi static pressure of 68.0 W at 45 K and 1.87 W at 4.2 K.

The PT420-RM units procured for SO have two minor customizations relative to the stock version sold by Cryomech. Additional bolt holes were added in both stages to provide better mating to the cryostat thermal shells, where the SO version has eleven M5 holes versus six holes in the standard unit. The second customization is a gold plated second stage cold head to improve thermal contact with the mating heat strap in the telescope. We expect the impact of these changes on the test results detailed here to be negligible when compared to similar units.

The PT420–1 was connected to its compressor via the 20-m helium lines provided by Cryomech, and it used the integrated motor driver in the Cryomech compressor. The remote motor option was chosen to reduce vibrational pickup in the cold heads. We mounted it on a separate plate using rubber offset feet that isolate the motor both electrically and vibrationally from the mounting surface. The compressor was delivered with a helium pressure level of 240 psi, which we did not adjust prior to testing. However, the recommended pressure for a 60 Hz system is 220 ± 5 psi. The manufacturer has indicated the increase in pressure may provide a small improvement in cryogenic performance, but it will primarily impact the power draw from the compressor. The magnitude of the effect can be seen by comparing our data to the manufacturer's data in Fig. 2. We also performed a test to examine the impact on a different PT-420 system by changing the pressure from 233 to 240 psi, which yielded $<$ 3% improvement on the first stage heat lift and a smaller change in capacity on the second stage of $<$ 1% for the higher pressure setting. We chose to operate at the higher pressure as the system will ultimately operate on a 50 Hz electrical grid, which requires 260 ± 5 psi for best performance as specified in the Cryomech user manual.

2.2. Testing chamber

The vacuum chamber utilized for the tests was originally the front section of the Microwave Bolometric Array Camera (MBAC) [13]. We repurposed a small section of the original camera along with the front and back vacuum plates of the receiver to make a cylindrical vacuum chamber 28 cm long with a diameter of 95 cm. The PT420–1 was mated to the chamber through an existing port combined with an adapter

[1] Cryomech Inc., Syracuse, NY

collar. A second port was also modified to allow attachment of an ISO-100 Accu-Glass[2] hermetic feedthrough (50D2-L100) with two D-sub 50 (DD-50) ports. The modified vacuum chamber is referred to hereafter as mini-MBAC (mMBAC). Heater wires used to load the separate stages occupied one of the DD-50 feedthroughs while the second DD-50 feedthrough was used for thermometry. The remote motor was mounted to an adjustable shelf attached to a metal frame that was used to stabilize mMBAC during testing. The motor head and the two ballast tanks were connected to the cold head with flexible stainless steel lines.

A radiation shell was installed around the second stage of the PTC to decouple the stage from the radiative environment. A 6061-T6 1/2" thick aluminum plate was attached to the first stage of the installed PTC to form the top of the radiation shield. A 6061-T6 1/2" thick aluminum box was bolted to the plate to complete the shield. The box had a slit to allow wires to pass to the second stage and was wrapped in a multi-layer insulation (MLI) blanket composed of 10 individual layers. The estimated radiative loading on each stage is < 1 W and < 1 mW, respectively. The ambient loading from radiation are small in comparison to the loading applied from heaters for our set points. We ignore ambient loading from the PTC itself since it is intrinsic to the device. See Fig. 1 for additional details of the test setup and the following section for information on the thermometers and heaters setup.

2.3. Heat application and temperature measurement

Heaters and thermometers were attached to both stages of the PT420–1 to characterize the performance of the unit. Parameters for the heaters were chosen to cover the range of power advertised for the units from Cryomech, as well as to cover the expected loading in the SO cameras and similar cryogenic setups. The design parameters from these inputs motivated loading values in the range of 0 to 55 W for Stage 1 and 0 to 1.8 W for Stage 2.

The first stage had a bank of five 100 Ω heaters connected in parallel (total resistance of 20 Ω) with fine gauge copper wires routing directly to a solder cup DD-50 connector. A power supply unit (PSU) with two 30 V outputs connected in series was used to drive these heaters, providing a maximum loading of 180 W. For the second stage, we clamped a 500 Ω heater against the bottom of the cold head. The heater was connected to the same DD-50 hermetic feedthrough via fine gauge copper wires routed to the 30 V channel on a second PSU that could provide a maximum load of 1.8 W. The estimated loading from wiring on each stage is < 0.3 W and < 1 mW, respectively. The loading are negligible compared to the loads from the heaters; however, we have accounted for them in the error bars in the analysis.

We used Lakeshore[3] DT-670 silicon diodes mounted in custom copper bobbins developed for use within SO. The diodes have an advertised precision of about 22 mK on the first stage and 12 mK for the second stage. The uncertainty on our temperature measurements was dominated by oscillations in the cold head temperature itself and not by the thermometer performance. A cryogenic breakout board (CBOB) developed for SO was used to convert an input 50 pin micro-D miniature (MDM-50) cable into twelve four-wire thermometer measurement connections. The CBOB allowed us to use existing manganin weave cables. We mounted the CBOB to a copper plate that was attached to the second stage cold head. Two diodes were bolted directly to the top copper surface of the PT420–1 first stage with wires routed to the CBOB on the second stage. An additional two diodes were bolted to the top of the second stage cold head and also connected to the CBOB. A 50 pin cable with a MDM-50 connector on one end and a DD-50 connector on the other was used to route the signal from the four thermometers to the hermetic DD-50 connector.

[2] Accu-Glass Products, Inc., Valencia, CA 91355
[3] Lake Shore Cryotronics, Inc., Westerville OH 43082

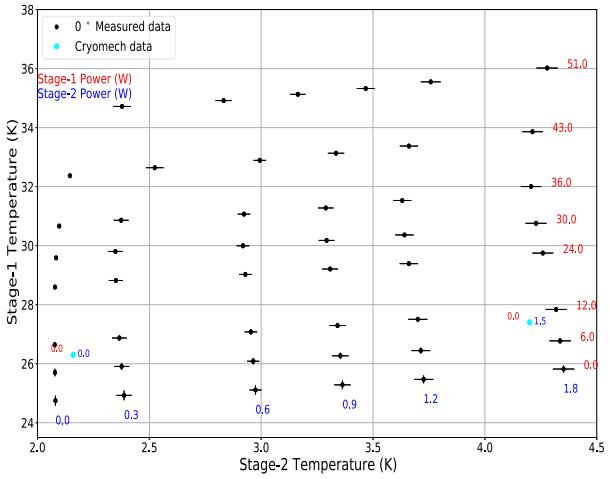

(a) 0° load curve

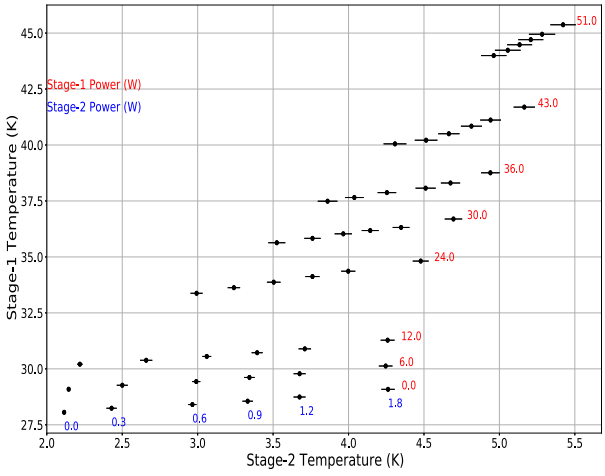

(b) 48° load curve

Fig. 2. PT420–1 load curve data at 0° (a) and 48° (b) with 0–51 W and 0–1.8 W on the first and second stage, respectively, forming an 8×6 grid. Two data points from the manufacturer are included in cyan in (a), which indicate performance differences between the Cryomech factory validation and our tests. We see 6–12 W of additional cooling power on stage-1 compared to the 0 W stage-1 data from Cryomech and a small improvement in capacity on stage-2. However, some difference is expected due to variations in the test cryostat used and the fact we operated our compressor at 60 Hz and 240 psi, while Cryomech operated theirs at 50 Hz and 260 psi. We also expect each PT-420 unit to have slight variations in performance.

2.4. Methodology

The cylindrical vacuum chamber made changing the angle relatively easy as we could roll the cryostat with the PTC installed to the desired angle. We attached a digital angle gauge to the top of the PT420–1 using the lab floor to zero the angle. We confirmed the setup gave us repeatable measurements to better than 1 degree. The remote motor and reservoir tanks were mounted on an adjustable shelf, which allowed us to rotate the test chamber without disconnecting the remote motor and reservoir tanks. Fig. 1 illustrates tilt directions for these tests.

We took data across an 8×6 grid over a range of power from 0–51 W on the first stage and 0–1.8 W on the second stage at 0°, 27.5°, 36°, 41°, and 48°. Fig. 2 displays the load curve at a couple of angles (0° and 48°), where the change in performance from one angle to another is conspicuous. We also took more detailed angular data at five power set points: $(P_1, P_2) = (0, 0)$ W, (0, 1.8) W, (24, 0.9) W, (51, 0) W, and (51, 1.8) W. We did not tilt beyond 60° due to physical limitations of our in-

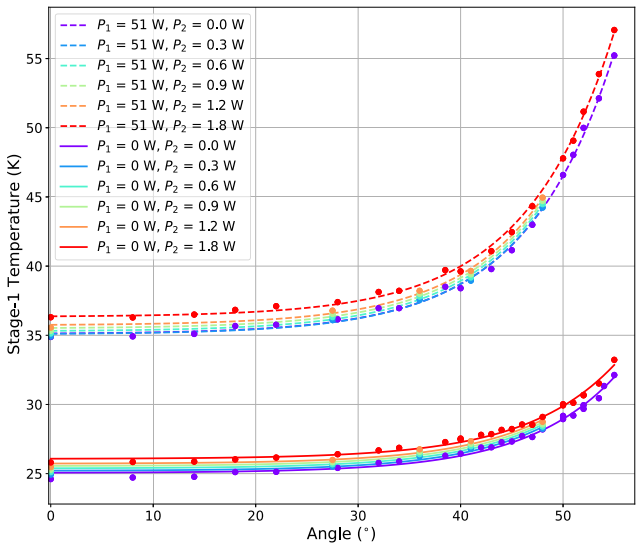

Fig. 3. Stage-1 performance and fit results for 0° (solid lines) and 51° (dashed lines). The fits are results from using Eq. 1 with parameter b_1 constrained to be the same for all power set points. Here we present performance of selected tilt test data at two extreme ends of power on the first stage.

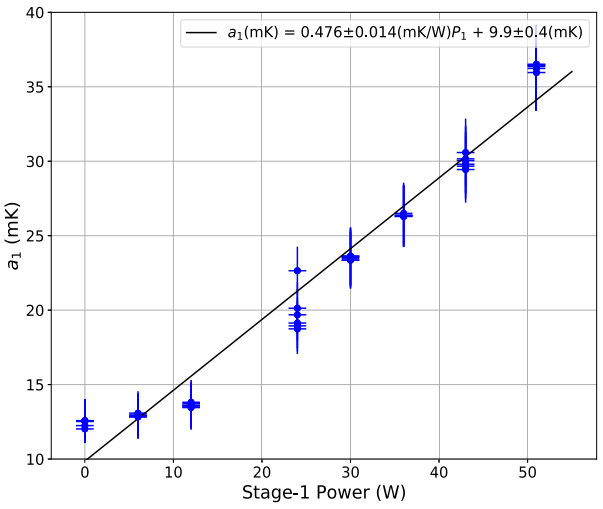

Fig. 4. Parameter a_1 vs Stage-1 power.

lab configuration.

We also rotated the test chamber in both positive and negative directions ($\pm\theta$) as well as around an axis perpendicular to the cylinder axis (backward tilt tests, ϕ) to explore dependencies of the PT420–1 on the axis about which it was tilted as the rotation axes were not symmetric with respect to the regenerators and pulse tubes as shown in Fig. 1.

The tilt-test load curves were obtained over a period of four weeks in November of 2019 in a highbay facility with fairly stable ambient temperatures that roughly follow the day night temperatures at UCSD. We did not observe any dependence on the diurnal cycle in our data.

2.5. Readout and Data Reduction

The diode thermometer four-wire measurements were performed using Lakeshore 240 Series Input Modules (LS-240s). LS-240s are programmable cryogenic readout instruments, each capable of simultaneously reading out up to eight independent voltage or resistance measurements down to 1 K. The diodes used for this analysis were calibrated by cooling them down on the same stage as a reference Lakeshore calibrated diode.

The LS-240s are connected via USB to a local computer, which records the temperature data to disk using the Observatory Control System (OCS) [14]. OCS is a distributed control system designed to coordinate data acquisition in astronomical observatories, and is used throughout SO for control and data storage across dozens of electronic devices[4]. The thermometry data was recorded at a rate of 1.6 Hz. PSUs were also controlled through OCS via ethernet to supply power to both stages. We operated them in current command mode, and at each loading step the current levels were set using the nominal resistance values of the stage heaters to supply an appropriate amount of power to each stage. To cycle through all the power set points, we applied power to the first stage and iterated through the second stage loading points. We then changed the power level on the first stage and repeated the process. A wait time was set between each change in loading to allow temperatures to stabilize. Steps on the first stage loading had a two hour wait time while changes on the second stage loading had a wait time of one hour. We iterated through all power set points before stepping the angle.

To obtain a single temperature value per step, per stage, we defined temperature stabilization criteria to select the range of data to be averaged. First, we found the extrema within the step in the direction the temperature was stabilizing. Then we selected all data after the temperature reached within 2% of the extrema, relative to the change between its minimum and maximum values during that step. In other words, we selected all data after the step was 98% "complete". We then applied a low pass filter to filter out the pulse tube intrinsic oscillation, where temperature fluctuated as a result of the adiabatic pressure oscillation in the pulse tube. Next, we selected the last 90% of the filtered section and calculated the median for the temperature data from this period to get a value and its associated uncertainty. The average temperature of the two thermometers on each stage determined by this method was used in the analysis.

3. Results

The extensive range of data we collected allows us to empirically constrain the performance of the PT-420–1 two stage PTC. We combined the high density load curve data at sparse angles (0 −48°) with the sparse load curve data with more detailed angular sampling (0 −55°) as shown in Fig. 3 and Fig. 5. The parameter space of the data with angular information combined with the loading and temperature at two stages presents a number of potential combinations for analysis. For simplicity we separate the data by stage and by power set points to compare temperature versus tilt angle. The following sections detail the results from the PT420–1 data.

3.1. Quantifying performance versus inclination angle

We empirically fit the data to an exponential function,

$$T_i(\theta) = a_i e^{b_i \theta} + c_i \quad (1)$$

where i is either 1 or 2 corresponding to the first and second stages, respectively. This formula provides a simple method to extract temperature from a given loading condition and tilt angle over the range we tested. The fit has an offset value c_i, which can be determined from the high density load curves at 0° (see Fig. 2), and it is equivalent to the temperature shift from extra loading at 0°. We utilize a parameter b_i in the model as a scaling of the angular dependence in the exponential that we leave fixed over our range of heat loads. The a_i term serves as a scaling parameter that can be fit as a function of the loading on the stage.

3.1.1. First stage fitting

We constrain b_1 using a least-square minimization fitting method,

[4] OCS Github: https://github.com/simonsobs/ocs

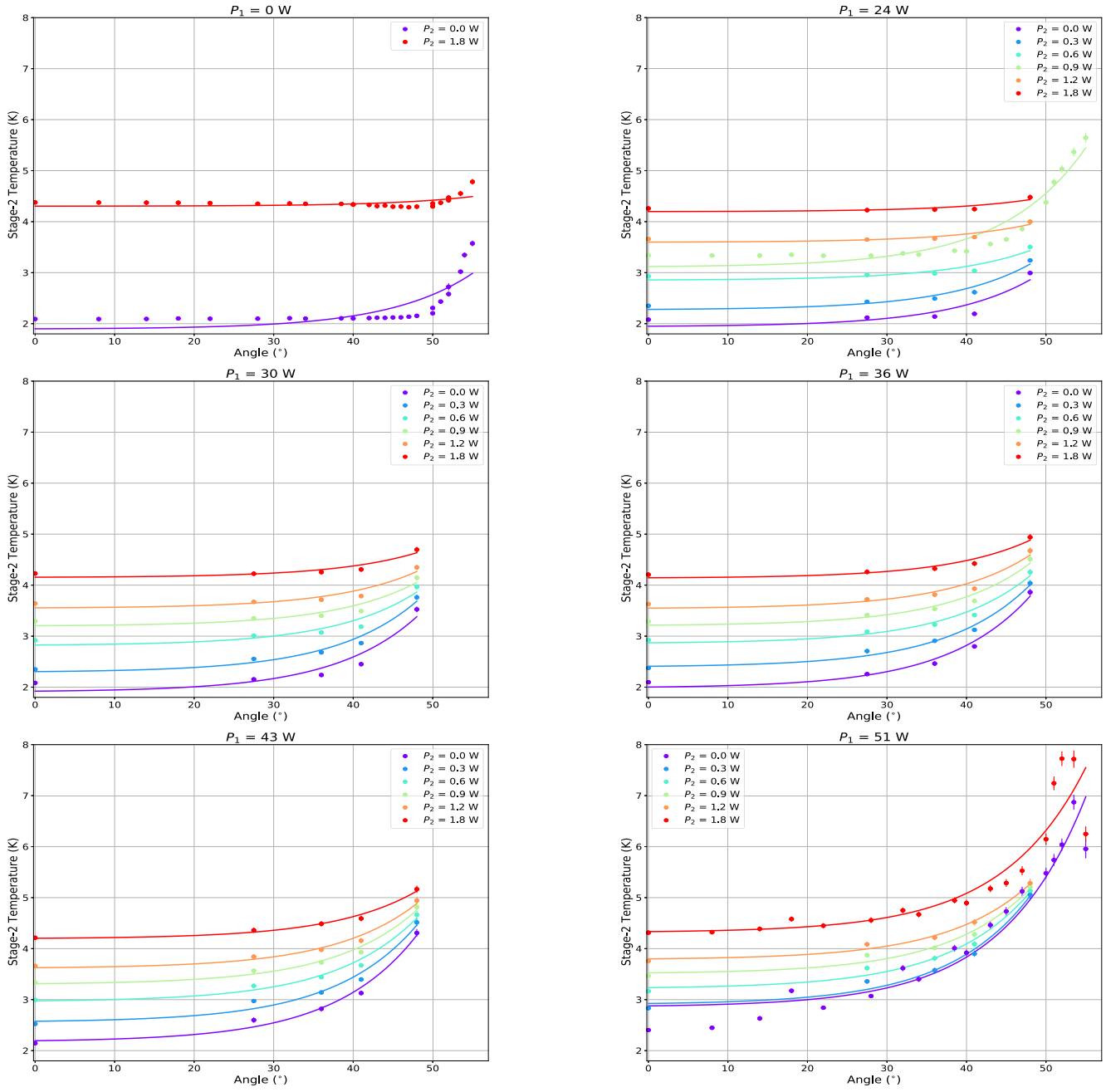

Fig. 5. Stage-2 performance and fit results (solid lines) using Eq. 1 with parameter b_2 constrained to be the same for all power set points. Here we include the tilt test data with fine angular sampling ($-\theta$) and the high density load curves with sparse angular sampling. The data sets with sparse angle information for the $P_1 = 0$ set point are excluded as the response was flat over the angular range examined, resulting in an inability to fit an exponential function to that data. We also excluded the sparse angle data for $P_1 = 6$ W and $P_1 = 12$ W due to their similarly flat response.

which allows it to remain independent of loading set points. This method fits all data sets at once with the condition that b_1 stays the same throughout while a_1 and c_1 are fit to the data for each power set point, effectively fitting 97 free parameters. We found the best-fit value of $b_1 = 0.1152 \pm 0.0013(deg.^{-1})$. Fig. 3 shows that the first stage performance is well fit by an exponential function across the sampled parameter space. As expected, a_1 exhibits a strong dependence on the first stage loading. A linear fit of a_1 versus first stage loading (Fig. 4) allows the determination of the a_1 parameter from a given loading value. The c_1 parameter can be determined by interpolation of the dense load curves shown in Section 2.4. We also note that the second stage loading primarily creates an offset at the 0° temperature for stage-1 which is captured in c_1. We do not attempt to separate the stage 2 loading effect on the shape of the stage 1 exponential as our data set is insufficient to determine significant trends.

3.1.2. *Second stage fitting*

We use the same empirical model and fitting procedure to analyze the second stage data. Stage-2 exhibits a strong dependence on both the first and second stage loading values, which makes it more challenging to fit with a simple exponential. As such, the empirical model is less effective for the second stage, but it is still useful in describing the system (see Fig. 5). In particular, the data from set points with $P_1 = 0$ exhibits unusual behavior that is not well fit by an exponential. For these points, the rise in temperature with angle is steeper and occurs at high angles, which meant the sparse angle data at this set point could not be

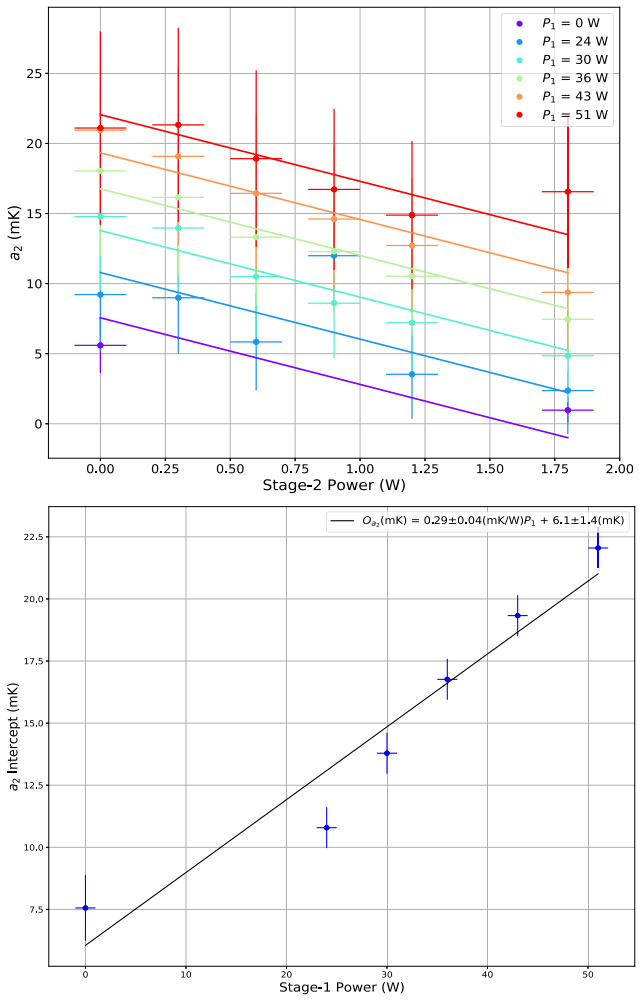

Fig. 6. Characterization of a_2. Top: a_2 as a function of P_2 with colors corresponding to different P_1 values. The linear fits all have the same slope allowing us to use the fit intercepts to decouple the first stage dependency. Bottom: The intercept values from the linear fits in the top figure plotted against P_1 with a second linear fit used to complete the empirical model for a_2.

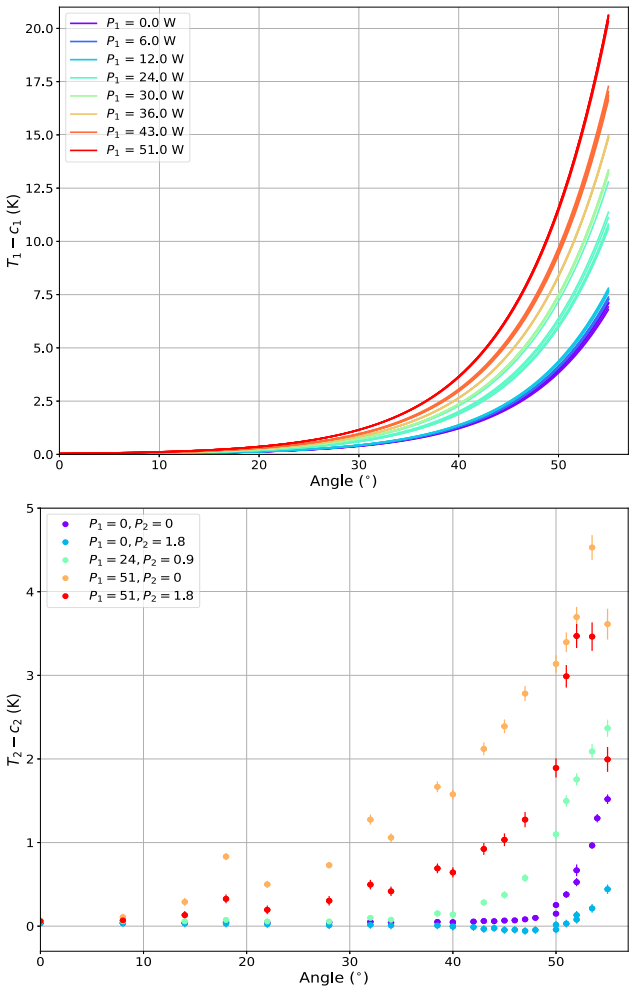

Fig. 7. Temperature Uniformity on both stages. The top and bottom plots show stage-1 fit functions and stage-2 detailed angular data, respectively, with the offset parameter c_i removed. The top plot has the fits for every power set point shown in Fig. 3, with the different stage-1 powers color coded from purple ($P_1 = 0$ *W*) to red ($P_1 = 51$ *W*). The spread in the line of each color is from the changing stage-2 powers, which has a small effect on the overall trend. The bottom plot portrays the stage-2 detailed angular temperature data as the second stage fits are less effective at capturing the trends at higher angles. However, the inverse relationship of a_2 with P_2 can be seen in the $P_1 = 0$ *W* and $P_1 = 51$ *W* set points which results in a wider angular range of Stage-2 temperature uniformity with increased P_2. (For interpretation of the references to colour in this figure legend, the reader is referred to the web version of this article.)

used as the response was flat across the $0-48^{\circ}$ range. We did not include the sparse angle data for $P_1 = 6$ W and $P_1 = 12$ W for the same reason. Overall, there were 65 free parameters fitted to the second stage data, and we found the best fit value of $b_2 = 0.096 \pm 0.006 (deg.^{-1})$.

The a_2 term displays a dependency on the loading from both stages. We develop a simple process to decouple the two power contributions to complete our empirical model. First, we fit a_2 as a function of P_2 with the slope, m_2, fixed for all P_1 set points, while letting the intercept float. The intercept is then plotted against P_1 to determine the dependence on the first stage power as shown in Fig. 6. The end result is:

$$a_2(P_1, P_2) = m_2 P_2 + d_2 P_1 + f_2 \tag{2}$$

d_2 and f_2 are the slope and intercept, respectively, of the fit to the a_2 fit intercept values versus P_1. From the fits, we have $m_2 = -4.8 \pm 0.5$ mK/W, $d_2 = 0.29 \pm 0.04$ mK/W, and $f_2 = 6.1 \pm 1.4$ mK. The linear fits effectively decouple the first and second stage contributions, allowing us to complete our empirical model as a combination of exponential and linear fits to the data we obtained.

3.2. Temperature uniformity over tilt range

For many of the instruments that use PTCs over a wide angle range, such as telescope cameras on pointed platforms, a primary design goal is to reduce scan dependent temperature drifts. The data here clearly favor constant tilt angle scan patterns that are already employed by many instruments. However, it is worth examining the relatively stable temperature regime we observe across the loading steps and tilt angles.

3.2.1. First stage temperature uniformity

The first stage temperature inflection follows the expected trend, with more rapid temperature change versus angle as the first stage power is increased, as shown in the top plot of Fig. 7. The effect of the second stage loading on the first stage temperature uniformity is also observed to be small and sub-dominant to the first stage loading effects. For the range of data we sampled, we see a less than 2 K change in temperature up to tilt angles of 30°. For design requirements favoring temperature uniformity over wider tilt ranges, there is a clear preference for lower loading values on the first stage.

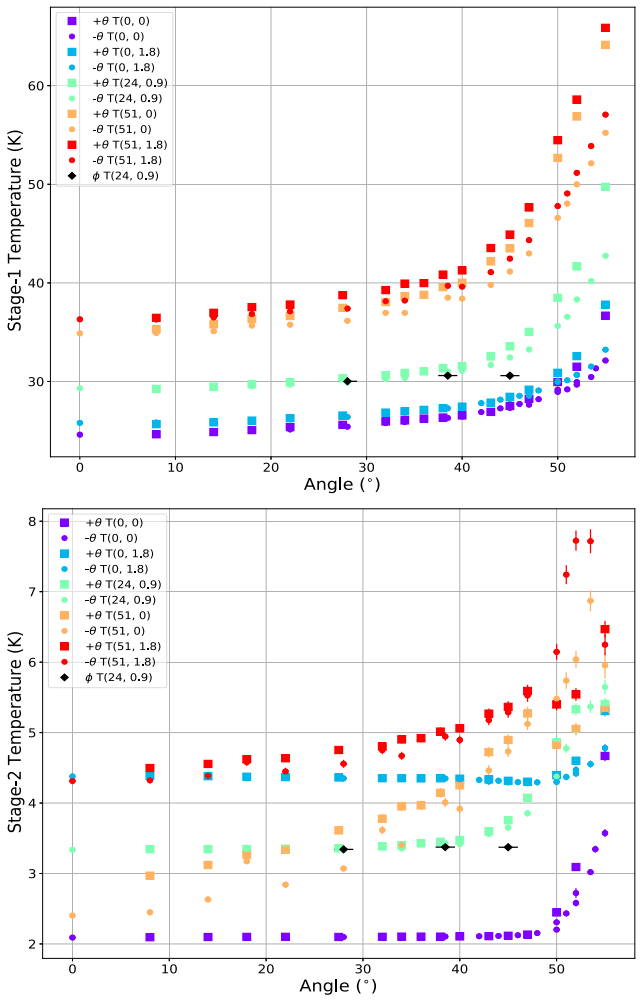

Fig. 8. Rotational Axis Dependence on both stages. Temperature data ($T(P_1, P_2)$) for the $+\theta$ (squares), $-\theta$ (circles), and ϕ tests (diamonds) are plotted as a function of angle. According to Stage-1 data, the dependency on tilt axis becomes prominent at high Stage-1 power and large tilt angle. This effect, however, is not as obvious on the second stage.

3.2.2. Second stage temperature uniformity

The behavior on the second stage is more complex given the second stage's cooling power is coupled to loading on both stages. As seen in the bottom plot of Fig. 7, the rate of temperature change increases with the first stage loading as one might expect. However, for the two sets with fixed first stage loading we see the increase in second stage loading actually produces a slower rate of temperature change with angle. The trend is also seen in the sparse angular data shown in Fig. 5, though it would be useful to have more detailed data at higher angles to confirm our finding. The behavior is also captured by the a_i slopes, where a_1 increases with P_1 as expected but a_2 has the opposite trend, decreasing with increased P_2.

The fact that the second stage trends are more closely tied to the first stage loading offers an important design input for projects, which favor a wider angular range of temperature uniformity on the second stage. The widest regime of minimal temperature change versus inclination angle is achieved with low power on the first stage but higher power on the second stage. The trend suggests that for best temperature uniformity over a tilt range there is a preference to decrease the first stage loading over decreasing the second stage loading.

3.3. Rotational axis dependence

The geometry of a two stage PTC is not symmetric about the primary central axis with regard to each stage's pulse tube and regenerator layout as shown in Fig. 1. To explore whether this asymmetry produces a rotational axis dependent effect of inclination angle versus cooling capacity, we tilted the PT420–1 unit in two additional rotational directions. First we tilted the chamber in the opposite direction from 0°, in the $+\theta$ direction, primarily affecting the relative orientation of the first stage pulse tube and regenerator. Second we tilted the unit backwards along a rotational axis, ϕ, perpendicular to the θ axis which primarily affects the second stage pulse tube and regenerator relative orientation. The results of these tests as compared to the primary rotation direction are shown in Fig. 8.

The data suggest a divergence between $\pm\theta$ on the first stage at higher angles and higher powers, favoring the $-\theta$ direction where the regenerator becomes lower than the pulse tube. However, additional data is needed to determine the magnitude of this trend. The backward tilt tests in ϕ are consistent with the other tilt directions which could be due to the fact that the second stage pulse tube is longer and narrower compared to the first stage pulse tube, which could reduce the impact of tilting in ϕ as the rotation primarily changes the orientation of the second stage components [15]. However, the challenges of tilting in that direction produced too sparse a set to fully explore the dependency.

4. Conclusions

Cryogenic cooling techniques have become prominent in telescope instrument applications as well as other branches of physics. Characterization of these cryogenic components is critical to guide instrument designs and ensure the achievement of science goals. We examined the performance of a Cryomech two-stage pulse tube cryocooler and produced an empirical model to quantify its cooling capacity. Given an expected loading on each stage, P_1 and P_2, the projected temperatures on each stage, T_1 and T_2, can be produced over a range of angles, θ, from 0 to 55 degrees using the following relationships:

$$T_1(\theta, P_1, P_2) = a_1(P_1)e^{b_1\theta} + c_1(P_1, P_2) \tag{3}$$

$$a_1(P_1) = 0.476(mK/W)P_1 + 9.9(mK) \tag{4}$$

$$T_2(\theta, P_1, P_2) = a_2(P_1, P_2)e^{b_2\theta} + c_2(P_1, P_2) \tag{5}$$

$$a_2(P_1, P_2) = -4.8(mK/W)P_2 + 0.29(mK/W)P_1 + 6.1(mK) \tag{6}$$

Where c_1 and c_2 can be produced by interpolating the load curve data at 0°. The exponential terms are $b_1 = 0.1152 \pm 0.0013(deg^{-1})$ and $b_2 = 0.096 \pm 0.006(deg^{-1})$ for the first and second stages, respectively. All the data sets, including the load curve for interpolation and fit results, can be accessed on github [5].

We found that the first stage performance versus angle is dominated by loading on the first stage and shows little to no dependence on the second stage loading over the ranges we explored. The first stage exhibits higher temperatures and a stronger angular dependence as more loading is applied. The second stage performance is more complex as its cooling capacity is dependent on the state of the first stage. The second stage tends to increase in temperature and exhibit a stronger angular dependence as more first stage loading is applied. However, we see evidence of decreased angular dependence as more power is applied on the second stage, producing an inverse relationship. This effect suggests designs that optimize second stage temperature uniformity rather than absolute temperature would benefit most from higher second stage loading and lower first stage loading.

[5] Data GitHub: https://github.com/ttsan2521/Cryomech_PT420_Data.git

We also performed tilt angle tests to probe any axial dependence of the tilt direction. The tests suggest slightly lower first stage temperatures when tilting in the $-\theta$ direction, while we did not see any significant dependence on the second stage. However, the data we obtained to explore this effect could be improved with more extensive measurements that explore a wider range of axial tilt directions and tilt angles than what we did in our tests.

The angular data sets we collected within our experimental time constraints were sufficient to construct a basic empirical model. However, the performance characterization of low-frequency two-stage PTCs would benefit from potential future investigations including measurements with more detailed load curve at each angular step over a larger range of angles, which could be used to construct a more complete empirical picture or be used to inform an analytic model.

Declaration of Competing Interest

The authors declare that they have no known competing financial interests or personal relationships that could have appeared to influence the work reported in this paper.

Acknowledgements

This work was funded by the Simons Foundation (Award #457687, B.K.). Support from the Ax Center for Experimental Cosmology at UC San Diego is gratefully acknowledged. Zhilei Zu is supported by the Gordon and Betty Moore Foundation.

References

[1] Gifford WE, Longsworth RC. Pulse-Tube Refrigeration. Journal of Engineering for Industry 1964;86(3):264–8. 08.
[2] Radebaugh R. Development of the pulse tube refrigerator as an efficient and reliable cryocooler. In: In London: IIR, volume 96 of Proceedings of the Institute of Refrigeration; 1999–2000.. p. 11–31.
[3] P. Goutham Raj, Animesh Biswas, and Subrata Kr. Ghosh. Phasor analysis of two-stage gm-type pulse tube refrigerator. In Special Issue 3: ICERTSD 2013, volume 3, pages 376–381, February 2013.
[4] Thummes G, Schreiber M, Landgraf R, Heiden C. Convective heat losses in pulse tube coolers: Effect of pulse tube inclination. In: Cryocoolers 9. Proc. 9th International Cryocooler Conference, Waterville Valley, NH, USA. New York: Plenum Press; 1997. p. 393–492.
[5] C. Wang and P.E. Gifford. Development of 4 K pulse tube cryorefrigerators at cryomech. In Susan Breon, Michael Dipirro, David Glaister, John Hull, Peter Kittel, Radebaugh Ray Pecharsky, Vitalij, Jay Theilacker, Steven van Sciver, II Weisend, John, and Albert Zeller, editors, Advances in Cryogenic Engineering CEC, volume 47 of American Institute of Physics Conference Series, pages 641–648, May 2002.
[6] Wang C, Gifford PE. A single-stage pulse tube cryocooler for horizontally cooling hts mri probe. AIP Conf. Proc. 2004;710(1):1805–11.
[7] Ross R, Johnson D. Effect of gravity orientation on the thermal performance of stirling-type pulse tube cryocoolers. Cryogenics 2004;44:403–8.
[8] Fang T, Mulcahey I, Spoor PS, Perrella MD, Conrad TJ, Ghiaasiaan SM. Investigation of gravitational effects in pulse tube cryocooers using 3-d cfd simulations. In: In Cryocoolers 19, International Cryocooler Conference Inc., Boulder, CO; 2016. p. 183–92.
[9] Nicholas Galitzki, Aamir Ali, Kam S. Arnold, Peter C. Ashton, Jason E. Austermann, Carlo Baccigalupi, et al. The Simons Observatory: instrument overview. In Proc. of SPIE, volume 10708 of Society of Photo-Optical Instrumentation Engineers (SPIE) Conference Series, page 1070804, July 2018.
[10] Ade Peter, Aguirre James, Ahmed Zeeshan, Aiola Simone, Ali Aamir, Alonso David, et al. The Simons Observatory: science goals and forecasts. JCAP 2019;2019(2):056. February.
[11] Choi SK, Austermann J, Basu K, Battaglia N, Bertoldi F, Chung DT, et al. Sensitivity of the Prime-Cam Instrument on the CCAT-Prime Telescope. J. Low Temp. Phys. 2020;199(3–4):1089–97. March.
[12] Kevork Abazajian, Graeme Addison, Peter Adshead, Zeeshan Ahmed, Steven W. Allen, David Alonso, et al. CMB-S4 Science Case, Reference Design, and Project Plan. arXiv e-prints, page arXiv:1907.04473, July 2019.
[13] Swetz DS, Ade PAR, Allen C, Amiri M, Appel JW, Battistelli ES, et al. Instrument design and characterization of the Millimeter Bolometer Array Camera on the Atacama Cosmology Telescope. In: volume 7020 of Society of Photo-Optical Instrumentation Engineers (SPIE) Conference Series; 2008. p. 702008.
[14] Brian J. Koopman, Jack Lashner, Lauren J. Saunders, Matthew Hasselfield, Tanay Bhandarkar, Sanah Bhimani, et al. The Simons Observatory: Overview of data acquisition, control, monitoring, and computer infrastructure. arXiv e-prints, page arXiv:2012.10345, December 2020.
[15] Risacher Christophe, Guesten Rolf, Stutzki Juergen, Hübers Heinz-Wilhelm, Buechel Denis, Graf Urs, et al. First supra-THz heterodyne array receivers for astronomy with the SOFIA observatory. IEEE Trans. Terahertz Sci. Technol. 2016;6:199–2016. December.